Effects of atmosphere on earth-space radio propagation

BY ODD GUTTEBERG

621.396.946

1 Topic

The growing demand for transmission capacity has forced the satellite telecommunication systems to use frequencies above 10 GHz. Systems are now operating at 11/14 GHz, and the utilisation of 20/30 GHz frequency band is being planned. At these frequencies the radio waves will suffer degradation through the non-ionised part of the atmosphere, i.e. the troposphere. Particularly dominant is the attenuation and depolarisation due to rain and wet snow. In the high-latitude part of the Nordic countries, additional problems arise due to very low elevation angle to geostationary satellites.

All these factors contribute strongly to the design criteria for satellite systems, such as

- localisation of earth stations
- r.f power requirements
- antenna sizes
- capacity requirements, etc.

and the technical solutions to be used.

Our main goal in designing satellite systems, is that all offered services must have the quality and reliability the customers want.

This paper deals with the different aspects of slant path propagation problems encountered in high latitude regions, i.e. elevation angles less than 20 degrees, and frequencies above 10 GHz.

2 Introduction

Normally a satellite transmission link is down-link limited. Accordingly, the important equation in designing satellite systems is:

$$\left[\frac{C}{N}\right]_{down} = EIRP + \frac{G}{T} + \frac{1}{k} + \frac{1}{B} + L_o + L_a \qquad (1)$$

where

EIRP = Satellite effective isotropic radiated power
G/T = Earth station "figure-of-merit"
k = Bolzmann's konstant
B = Transmission bandwidth
L_o = Free space loss
L_a = Additional loss

All terms expressed in dB.

The time varying parameters are the additional loss (L_a) and the earth station system noise temperature (T). Earth station antennas without tracking will also have a decrease in gain (G) due to variations in angle of arrival.

The major tropospheric propagation factors that will influence satellite communications are;

- absorption due to atmospheric gases
- radio ray bending due to the decrease in refractive index with height
- scattering due to atmospheric turbulence
- attenuation due to rain
- depolarisation due to rain and snow
- radio noise due to attenuation in gases and rain.

Basic considerations and reviews are found in [1-4]. In the following chapters measurement of the different effects will be presented, bearing in mind the system planners' need for prediction models.

3 Atmospheric absorption

Radio wave absorption is due to gaseous constituents in the atmosphere, primarily water vapour and oxygen.

In order to calculate the total slant path attenuation, we need the specific attenuation (γ), and the equivalent height (h) for water vapour and oxygen, see figures 1 and 2.

According to CCIR [4] the equivalent heights are;

h_o = 6 km for oxygen for frequencies below 50 GHz

h_w = 2.2 - 2.5 km for water vapour in the frequency range 10 - 20 GHz

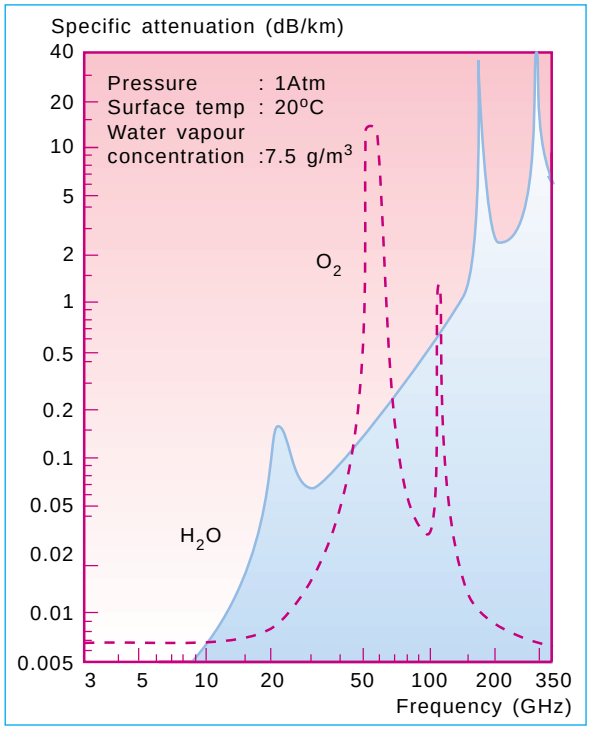

Figure 1 Specific attenuation due to oxygen and water vapour in the atmosphere [1]

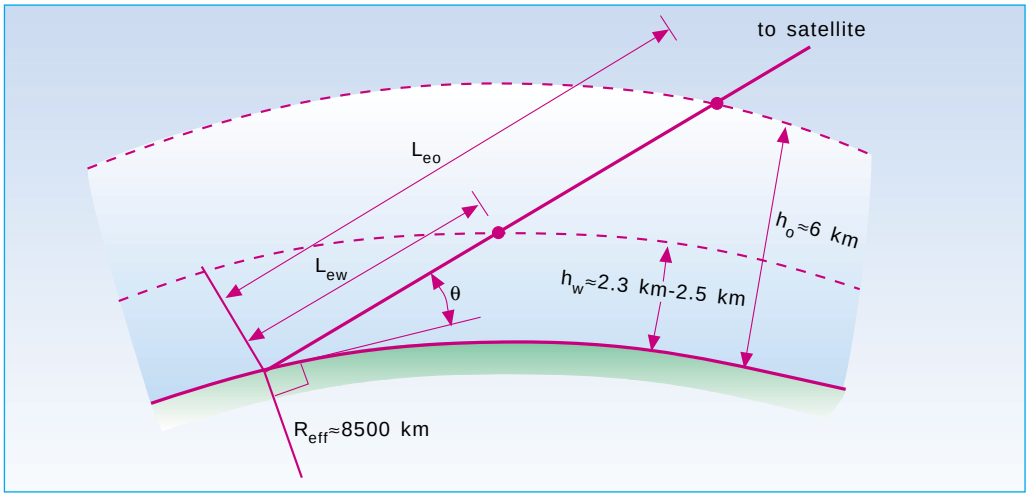

Figure 2 Parameters for calculating the total slant path atmospheric absorption
θ = elevation angle
h = equivalent height of water vapour (h_w) and oxygen (h_o)
R_{eff} = effective earth radius = 8,500 km

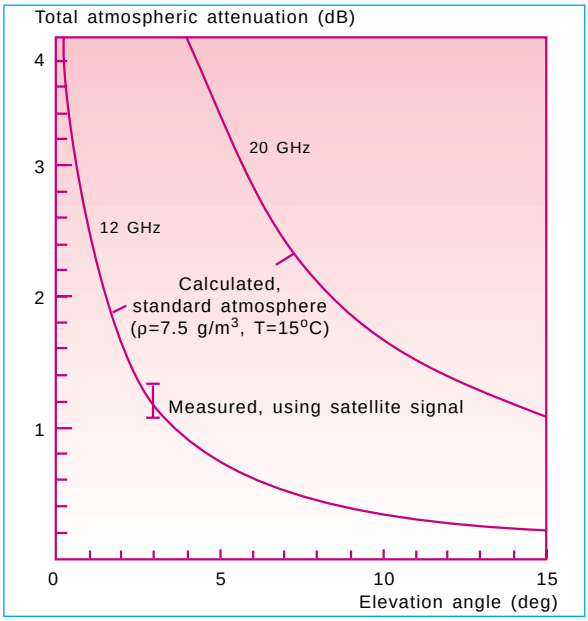

Figure 3 Total atmospheric attenuation as a function of elevation angle for a standard atmosphere (15° C temperature, 7.5 g/m3 water vapour density). Measured value at 3° elevation angle is indicated

The total attenuation can then be calculated;

$$A = \gamma_o \cdot L_{eo} + \gamma_w \cdot L_{ew} \ (dB) \qquad (2)$$

where the equivalent path length is found from geometric considerations, figure 2:

$$L_e = \frac{2h}{\sqrt{\sin^2\theta + \frac{2h}{R_{eff}}} + \sin\theta} \qquad (3)$$

Using this approach, the atmospheric attenuation for 12 and 20 GHz has been calculated as a function of elevation angle, figure 3. A standard atmosphere is assumed, i.e. ground temperature of 15° C and water vapour density of 7.5 g/m^3.

As can be seen, the attenuation for 12 and 20 GHz are less than 1 dB for elevation angles down to about 3° and 15°, respectively. At very low elevation angles, the atmospheric absorption will become a critical design factor.

From C/N-measurements of 12 GHz satellite signals at Spitzbergen (78° N, 3° elevation angle), the atmospheric absorption has been estimated. The measurements were performed with two satellites (OTS and EUTELSAT-I, F-2), and two receiving antennas (3 m and 7.6 m in diameter). At elevation angles less than 5°, defocusing loss and the decrease in antenna gain due to wave front incoherence will be of importance. For the actual antenna sizes and elevation angle, these effects are estimated to 0.7 - 0.9 dB [4]. Taking this into account, the satellite signal measurements showed an atmospheric absorption of 1.1 - 1.3 dB at 3° elevation, figure 3.

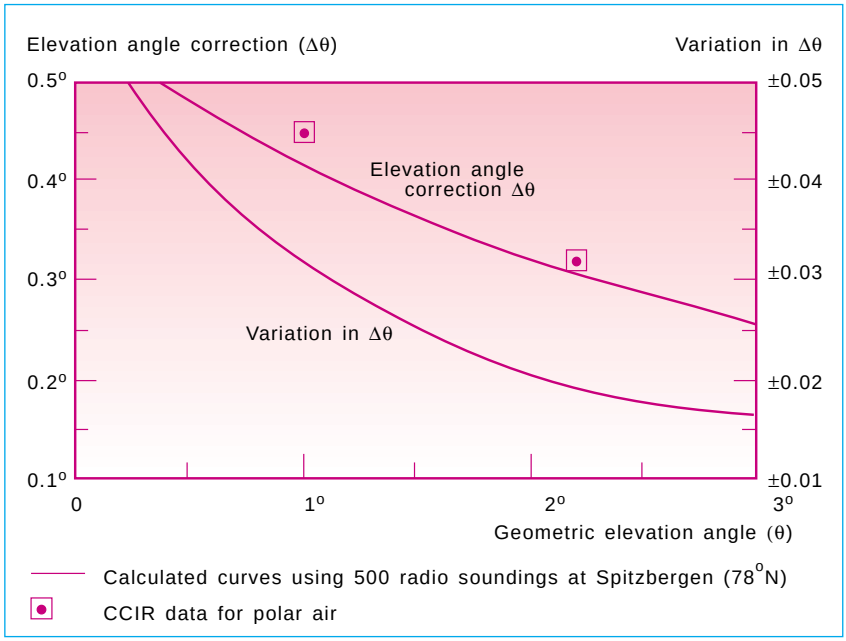

Figure 4 Average ray bending in polar areas

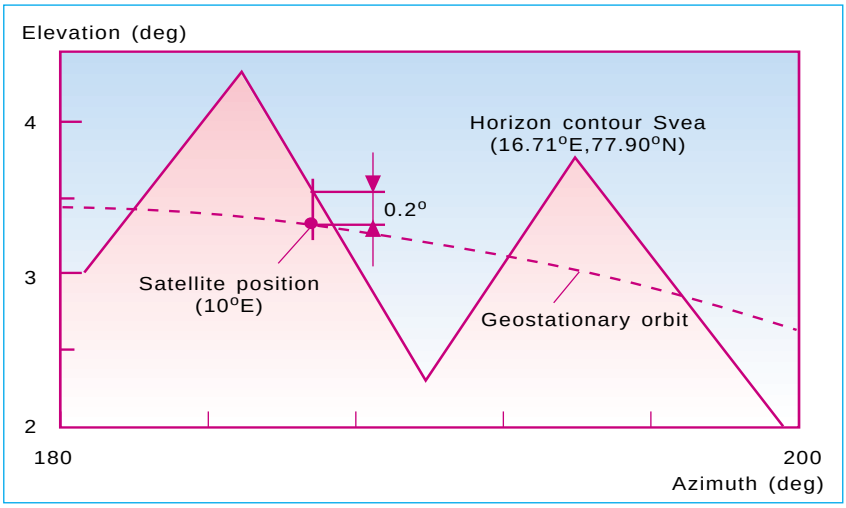

Figure 5 Horizon contour and geostationary orbit for Svea, Spitzbergen (16,71° E, 77,90° N)

This is quite close to the calculated value, which indicates that the model used for predicting the atmospheric absorption is reasonably good.

4 Angle of arrival

The decrease of refractive index with height, causes bending of radio waves. This means that the apparent elevation angle to a satellite will be greater than the geometric elevation angle. At very low elevation angles, the correction will be of the same order of magnitude as the elevation angle.

From 500 radio soundings at Spitzbergen (1960), the refraction profiles have been found [5]. The ray bending has been calculated, using the method described in ref. [6]. The results are shown in figure 4, together with data from CCIR [4].

As can be seen, there is good correlation between the calculated angle deviations and the CCIR data.

The normal refraction effect has been successfully utilised when receiving the satellite transmissions from EUTELSAT-1 (10° E) in Svea at Spitzbergen (77.9° N). Figure 5 shows the local horizon contour, and the geostationary orbit. The satellite is approximately 0.2° below the local horizon.

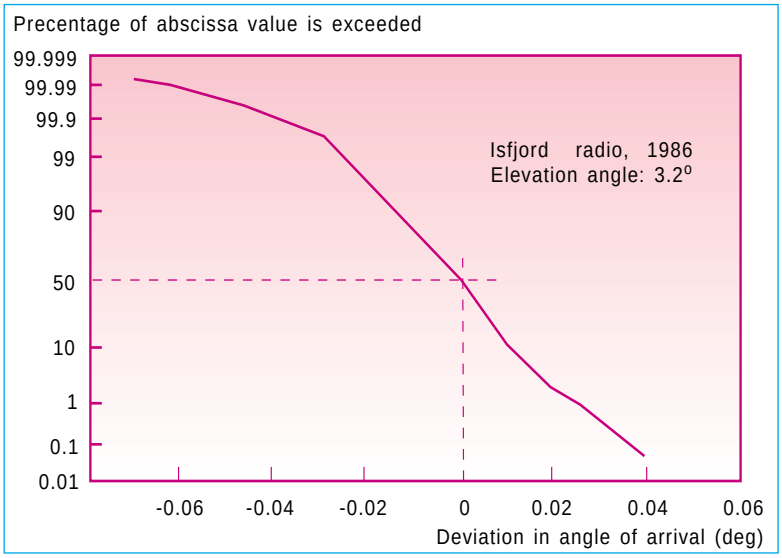

Figure 6 Cumulative distribution of angle of arrival measured at Isfjord Radio, 1986. Elevation angle 3.2°, frequency 11.5 GHz, mean ground temperature 4° C

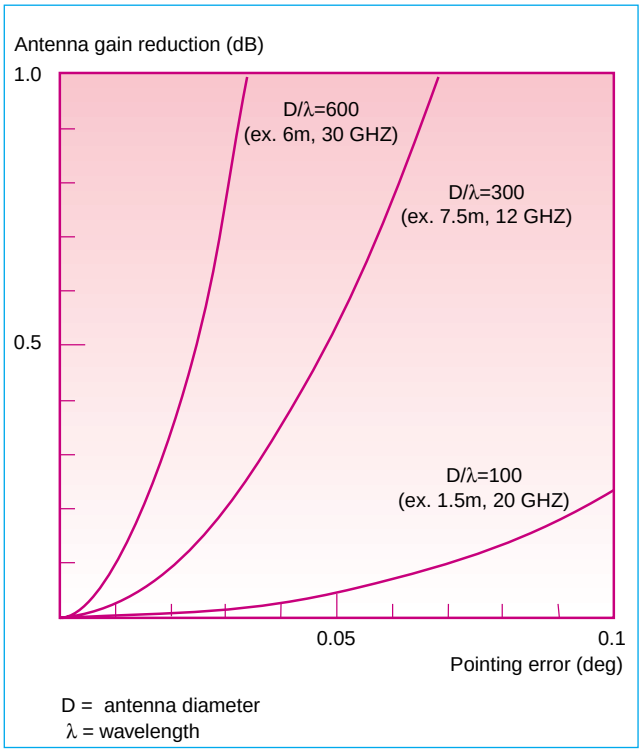

Figure 7 Reduction in antenna gain due to variation in angle of arrival

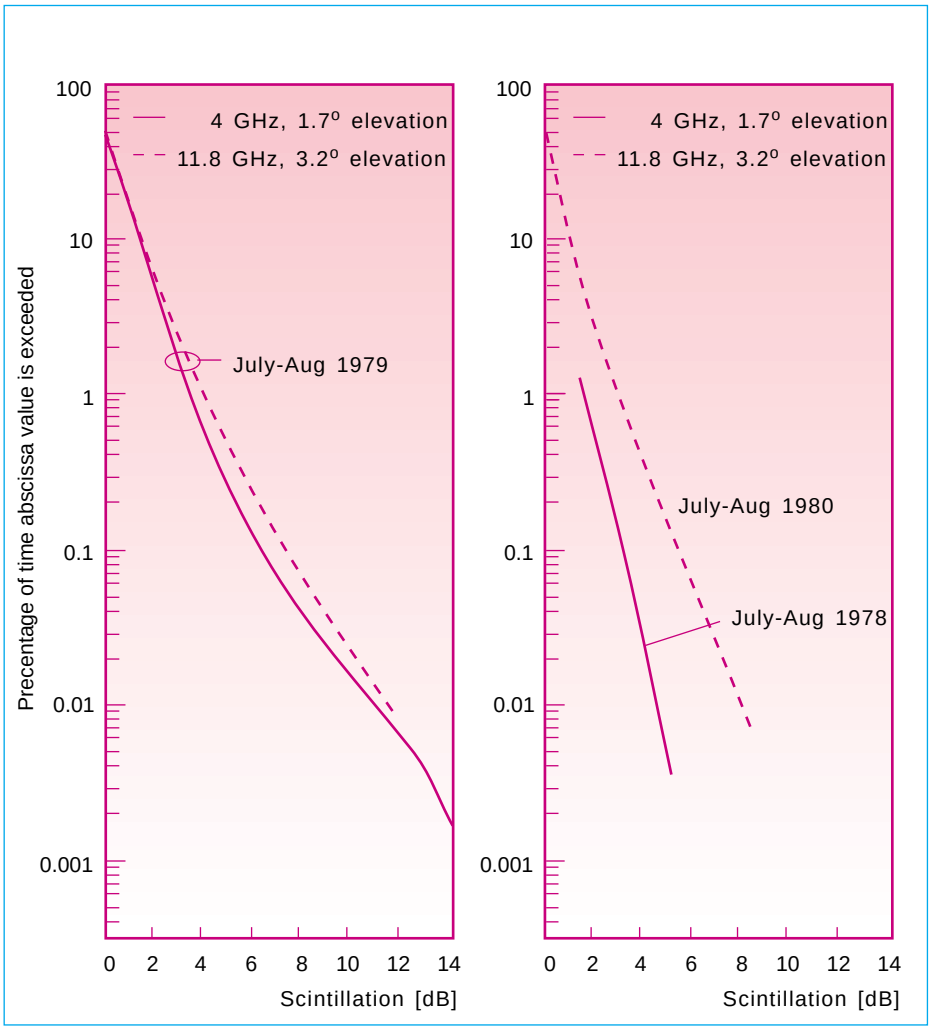

Figure 8 Measured scintillation distributions 4 and 11.8 GHz. Isfjord Radio, Spitzbergen, 1979

Figure 9 Measured scintillation distributions 4 and 11.8 GHz. Isfjord Radio, Spitzbergen, 1978 and 1980

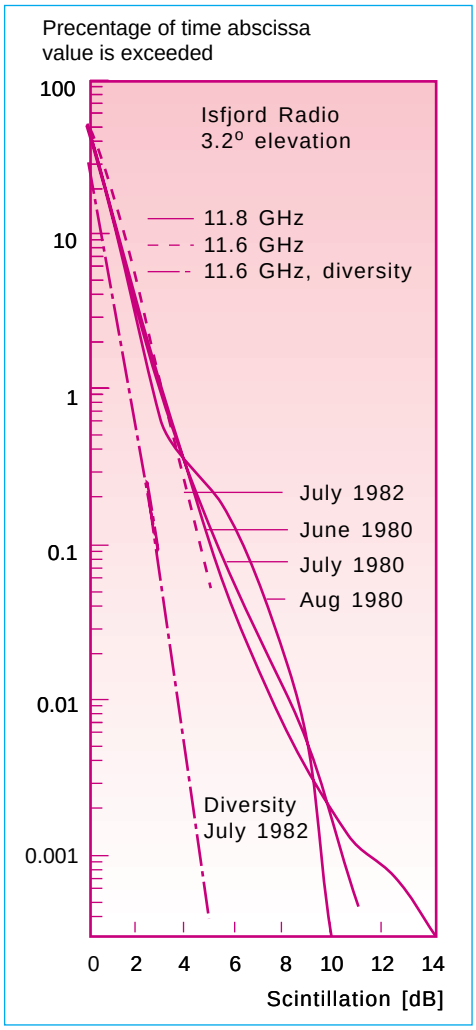

Figure 10 Measured scintillation distributions 11.8 GHz (1980 and 1982) and diversity (1982)

However, when taking into account the ray bending, the satellite will be seen above the local horizon.

Normally, the refractive index decays exponentially with height. Atmospheric turbulence will, however, cause random fluctuations about the average value of the refractive index. This results in random fluctuations in the apparent elevation angle to the satellite. This effect is important for earth stations operating at very low elevation angle without antenna tracking system.

Measurements of fluctuations in angle of arrival have been performed at Spitzbergen during summer 1986 [7] using the telemetry beacon of EUTELSAT-I, F-1 (13° E).

To obtain better accuracy, two 3-metres antennas were used, one pointing slightly above and the other below the nominal direction to the satellite.

The cumulative distribution of fluctuations in elevation angle is shown in figure 6. As can be seen, the deviations in angle of arrival is less than ±0.02° in 95 % of the time. The distribution is approximately Gaussian. The slow variation due to satellite movement was filtered out.

Figure 7 shows the reduction in antenna gain as a function of the pointing error. A fluctuation in the angle of arrival of 0.02° reduces the gain 0.8 dB for a 6 metre antenna at 30 GHz or 0.2 dB for a 7.5 metre antenna at 12 GHz.

5 Tropospheric scintillations

Amplitude scintillations are generated by refractive index fluctuations in the lower part of the troposphere (<1 km). The fluctuations are caused by high humidity gradients, and temperature inversion layers.

For very low elevation paths to high latitude regions with scarce amount of rain, e.g. polar areas, tropospheric amplitude scintillations are the dominating propagation effect.

Long term measurements of this effect have been performed at Spitzbergen both at 4 GHz (1.7° and 3.1° elevation angle) [5] ,and 12 GHz (3.2° elevation angle) [8, 9]. Examples of measured cumulative distributions are given in figures 8, 9 and 10.

The turbulence activity is increasing with rising temperature in the atmosphere. One should therefore, to a certain extent, expect a dependence between scintillations and the ground temperature. It has been shown that such a relationship exists [11].

From statistical measurements at Spitzbergen *(ε = 3.2°, f = 11.8 GHz)*, the following equation has been established:

$$A_{sci} = 0.27 \cdot T_g + 6 \text{ (dB)} \qquad (4)$$

where

A_{sci} = fading level for 99.99 % of a month

T_g = monthly mean ground temperature

Due to turbulence activity, the received signal will consist of a direct signal plus a scattered signal. If we assume that the scattered field consists of several components with random amplitude and phase, then the resulting signal distribution could be described by a Rice-distribution, i.e. a constant vector plus a Raleigh distributed vector.

In the measurements made at Spitzbergen, the scintillations were found to follow Rice-distributions with different values of the power ratio (K) of the random components to the steady component as given in table 1 [9].

According to the theory for turbulent scatter, the standard deviation of the scintillation amplitude is given by [4]:

	Worst day	Worst summer month	Average winter month
K	- 10 dB	- 13 dB	- 20 dB

Table 1

Measuring period	July/Aug 1979		July/Aug 1978 1980	
Frequency (GHz)	11.8	4	4	11.8
Elevation angle (°)	3.2	1.7	3.1	3.2
Antenna diameter (m)	3.0	4.5	4.5	3.0
G(R)	0.923	0.954	0.940	0.923

Table 2

Frequencies	11.8 / 4	11.8 / 4*
Elevations	3.2 / 1.7	3.2 / 3.1
Theoretical scaling factor	0.97	0.55
Average measured scaling factor	1.11	0.59

Table 3

**There are no simultaneous measurements of 4 and 11.8 GHz at 3° elevation angle. Since the average temperature for July/August 1978 and 1980 are approximately the same, the cumulative scintillation distribution for these periods are compared.*

$$\sigma(f,\theta,D) \sim (f)^{\frac{7}{12}} \cdot \left[\frac{1}{\sin\theta}\right]^{\frac{11}{12}} \cdot [G(R)]^{\frac{1}{2}} \quad (5)$$

where

f = frequency (GHz)

θ = elevation angle (degrees)

G(R) = antenna aperture averaging factor [4].

For the experiments at Spitzbergen, we have the technical data as shown in table 2.

The cumulative distributions of scintillations for the different measuring periods are shown in figure 8 and 9. Knowing one distribution, equation (5) can be used to scale this distribution to other frequencies and elevation angles.

A comparison of the theoretical scaling factors, calculated from equation (5), and the average scaling factors obtained from the measured distributions in figure 8 and 9, are given in table 3.

The measured values are in accordance with the calculated values. This means that the turbulence theory can be used with good accuracy for scaling a measured scintillation distribution to other elevation angles or frequencies.

To reduce the fading margin required for satellite links operating at very low elevation angle, space diversity may be employed. Site diversity measurements have been performed at Spitzbergen with a lateral separation of 1150 metres [9]. The single site and joint distributions are shown in figure 10. As can be seen, a substantial improvement is achieved. At a 3.2 dB fading level, the availability improves from 99 % to 99.9 %, due to site diversity. The diversity gain is 2 dB at 0.1 % of time. For smaller percentage of time, even larger diversity gain is expected.

6 Rain attenuation

Rainfall plays a major role in satellite communication, especially for systems operating above 10 GHz. A radio wave propagating through rain will be attenuated due to absorption, and scattering of energy by the water drops. The attenuation in dB per km (γ) is related to the rainfall rate (R) in mm/h. For practical applications this relationship can be written;

$$\gamma = a \cdot R^b \ (\mathrm{dB/km}) \quad (6)$$

where a and b are parameters depending on frequency and temperature [1]. Some values for a and b are given in table 4.

Since the rain intensity will vary along the path, the attenuation $A(t)$ is obtained by integrating the specific attenuation γ over the total path length l:

$$A(t) = \int_o^l \gamma dx \quad (7)$$

where

$$\gamma = f[R(x,t)]$$

Knowledge of the rainfall rate distribution in one point is generally not enough for calculating the attenuation distribution. To be able to predict the rain attenuation, we introduce the concept of “equivalent path length”, which is defined by;

$$A\ (dB) = \gamma \cdot l_{eq}$$

or

$$l_{eq} = \frac{A(p)}{\gamma(R(p))} \quad (8)$$

where $A(p)$ and $R(p)$ are the attenuation and rain rate exceeded for p percentage of time (equal-probability values).

The equivalent path length is found from simultaneous statistical measurements of rain attenuation and rainfall rate. This has been done at 12 GHz both at Kjeller [10], and Kirkenes [11], with elevation angles 22° and 10°, respectively. The measured equivalent path lengths are presented in figure 11. Linear interpolation has been used for calculating the equivalent lengths for intermediate values of the elevation angle.

When knowing the cumulative distribution of rainfall rate in one point, we are able to calculate the attenuation distribution by using equation (6) and figure 11. In Norway, rain intensity data from tipping-bucket gauges are available in more than 50 places and for several years, This information has been used to identify regions of different rainfall rate statistics, see figure 12.

The described prediction model has been used to calculate the 12 GHz rain attenuation distribution for;

- Zone A, elevation angle 11.5° (Tromsø)
- Zone A, elevation angle 18° (Trondheim)

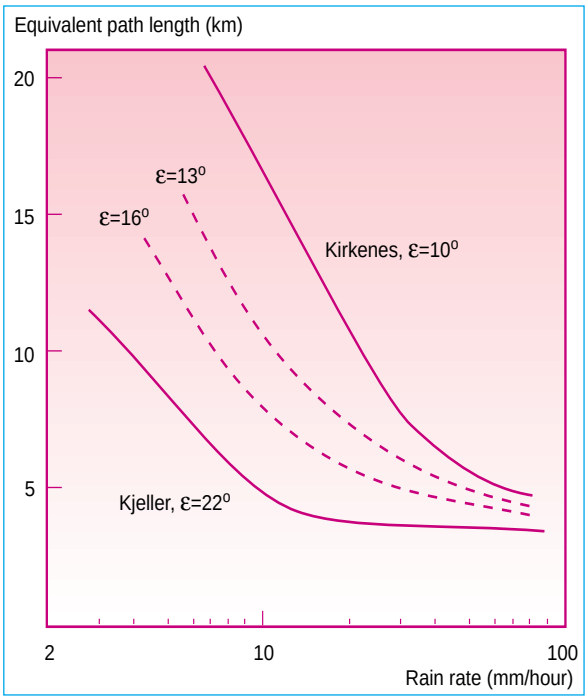

Figure 11 Equivalent path length through rain

Frequency (GHz)	Horisontal pol		Vertical pol	
	a	b	a	b
12	0.0188	1.217	0.0168	1.200
15	0.0367	1.154	0.0335	1.128
20	0.0751	1.099	0.0691	1.065
30	0.187	1.021	0.167	1.000

Table 4

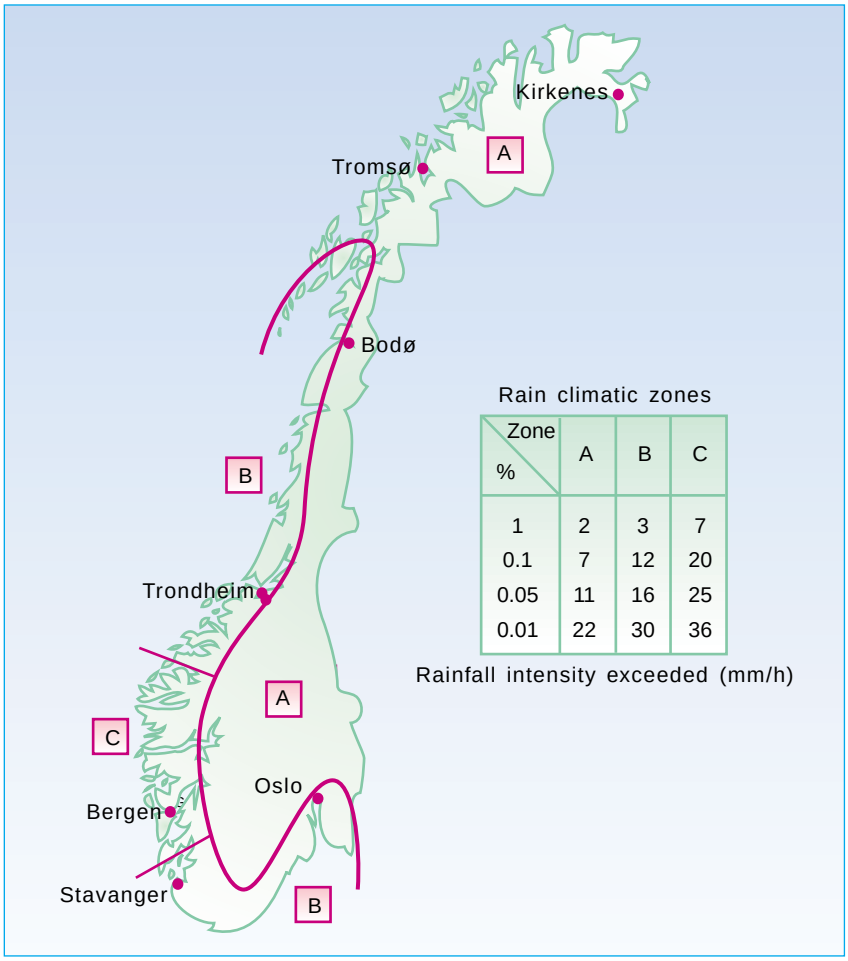

Figure 12 Rain climatic zones for Norway

- Zone C, elevation angle 21° (Bergen).

The predicted and measured distribution are compared in figure 13 and 14. As can be seen, the deviations are quite small, and within what is expected due to year-to-year variations of the rainfall rate.

As the equivalent path length is independent of frequency, attenuation distributions for other frequencies can be predicted. Figure 15 shows the calculated cumulative rain attenuation distribution for 20 GHz in Zone A, elevation angle 20°. The predicted attenuation is compared with attenuation results from the Helsinki 20 GHz radiometer [12]. Helsinki has approximately the same rain intensity climate as zone A. There is a reasonable agreement between the distributions.

The good correlation obtained between the calculated and measured rain attenuation distributions should demonstrate the usefulness of the described prediction procedure.

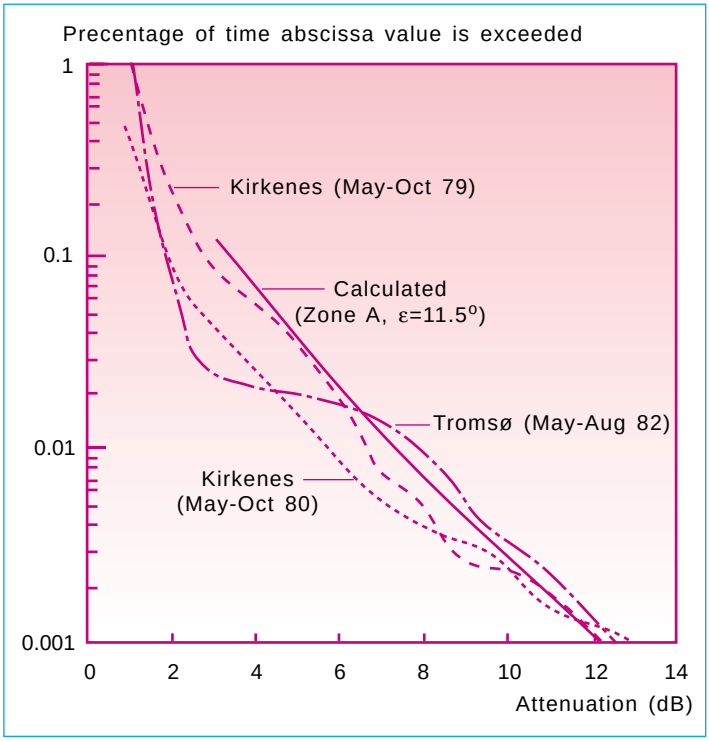

Figure 13 Cumulative distributions of rain attenuation measured in Kirkenes (ε = 10.5°) and Tromsø (ε = 11.5°). Calculated distribution for zone A (ε = 11.5°)

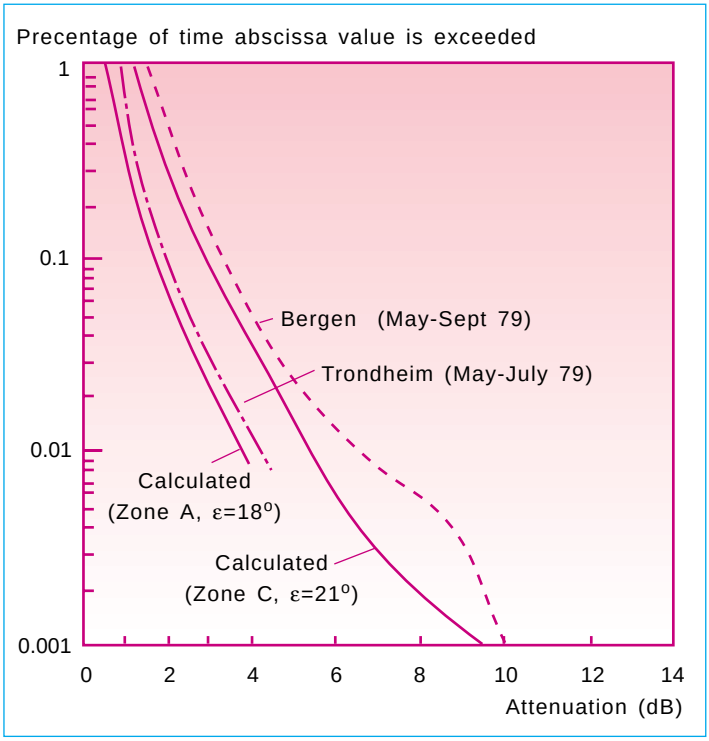

Figure 14 Cumulative distributions of rain attenuation measured in Trondheim (ε = 18°) and Bergen (ε = 21°). Calculated distributions for zone A (ε = 18°) and zone C (ε = 21°)

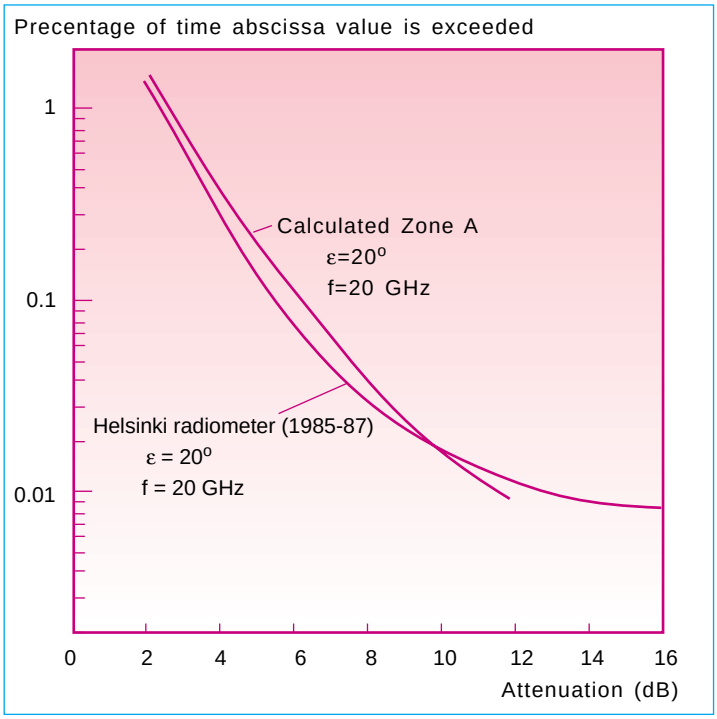

Figure 15 Cumulative distribution of 20 GHz attenuation measured with radiometer in Helsinki (zone A, e = 20°). Calculated distribution for zone A (e = 20°) including 0.8 dB gaseous absorption

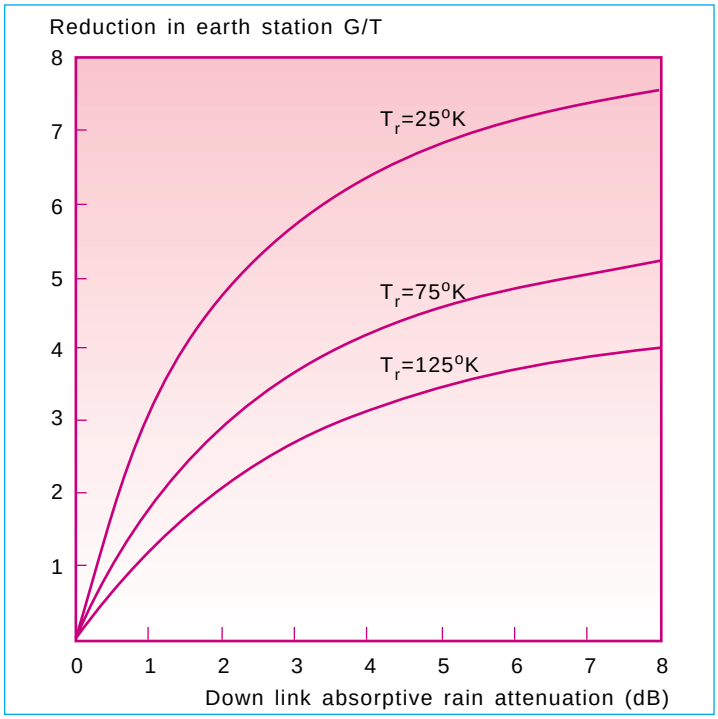

Figure 16 Reduction in earth station G/T as a function of the down link attenuation. Tr = receiver noise temperature. Clear sky noise temperature of antenna Tao = 25° K

7 Noise Temperature

Any absorbing medium, such as atmospheric gases and rain, will in addition to attenuating a radio signal produce thermal noise power radiation. This noise emission is directly related to the intensity of absorption. If we consider the atmosphere as an absorbing medium with an effective temperature of T_m and a loss factor of L, the contribution to the earth station antenna noise temperature T_a is given by;

$$T_a = (1 - 1/L)T_m \qquad (9)$$

T_m varies between 260 - 280° K depending on the atmospheric conditions.

An increase in antenna noise temperature will give a corresponding decrease in the earth station figure of merit *(G/T)*. As the clear sky system noise temperature decreases due to better performance of low noise front-ends and antennas, the decrease in *G/T* could be larger than the attenuation itself.

An example of the degradation in *G/T* as a function of down-link absorptive rain attenuation is given in figure 16.

The following values are assumed:

- Gaseous absorption: 0.2 dB
- Antenna ground interception factor: 3.5 % (NORSAT-B antennas)
- Effective absorbing medium temperature: 280° K.

This corresponds to a clear sky antenna noise temperature of 25° K.

The degradation of the down-link carrier to thermal noise ratio (dB) will be the sum of the reduction in *G/T* (dB), and the down-link attenuation (dB).

8 Cross polarisation

To increase the channel capacity, orthogonal polarisations can be employed. However, due to atmospheric effects, there will be a transfer of energy from one polarisation to another. This will cause interference in dual polarised satellite links. Depolarisations are mainly caused by rain and snow along the path.

Cross polarisation discrimination *(XPD)* has been measured at Kjeller and Spitzbergen. Figure 17 shows equi-probability plots of the *XPD*, and the copolar attenuation [8-10]. The depolarisations measured at Kjeller are caused by rainfall, whereas the depolarisations measured at Isfjord and Spitzbergen, are believed to be due to sleet, snow and/or atmospheric turbulence.

Due to the short measuring period at Kjeller (two summer months), there is a discrepancy between the predicted *XPD* (CCIR), which is based on long-term statistics, and the measured *XPD*.

Snow and atmospheric turbulence appear to be a less polarising medium than rain.

9 Snowfall Attenuation

Dry snow has little effect on frequencies below 30 GHz. Sleet or wet snow can, however, cause larger attenuation than the equivalent rainfall rate [10].

Along the North Atlantic coast of Norway, the intensity of wet snowfall is known to be high. Measurements at 12 GHz in Tromsø (70° N) showed that the “winter attenuation” was much larger than “summer attenuation” for the year 1982. Attenuation up to 15 dB due to sleet were experienced [11].

10 Conclusions

Prediction models for gaseous absorption, tropospheric scintillations and rainfall attenuation have been established. The described methods have successfully been used when designing commercial 11/14 GHz satellite systems in Norway, including Spitzbergen.

To a certain extent, these models can be utilised for planning of satellite systems in the 20/30 GHz band. Through the Norwegian participation in the propagation experiments with the OLYMPUS satellite, more reliable data of the atmospheric influence on satellite links will be established.

As the attenuation increases, different techniques have to be used in order to keep the fading margins to a minimum. These techniques include site diversity, power control, spot beams in the satellite and possibly adaptive allocation of system capacity.

11 References

1 Ippolito, L J. *Radio wave Propagation in Satellite Communications*, Van Nostrand Reinhold Co. Inc, New York, 1986.

2 Davies, P G, Norbury, J R. Review of slant path propagation mechanism and their relevance to system performance, *IEE Proceedings*, Vol 130, Part F, No 7, Dec 1983.

3 Davies, P G, Norbury, J R. Review of propagation characteristics and prediction for satellite links at frequencies of 10-40 GHz, *IEE Proceedings*, Vol 133, Part F, No 4, July 1986.

4 CCIR Recommendations and reports, Vol V. *Propagation in non-ionized media*, ITU, Geneva 1986.

5 Osen, O. *Propagation Effects in High Latitudes*, Symphonie Symposium, Berlin, 1980.

6 Schulkin, M: Average Radio-Ray Refraction in the Lower Atmosphere, *Proceedings IRE*, May 1952, 554-561.

7 Erring, B. *Variasjoner i innfallsvinkel for satelittkommunikasjon ved lave elevasjonsvinkler*, Hovedoppgave, NTH, Trondheim 1987.

8 Gutteberg, O. Measurements of tropospheric fading and crosspolarization in the Arctic using Orbital Test Satellite, *IEE Conference Publication* 1, No 195, Part 2, 71-75, IEE 2nd International Conference on Antennas and Propagation, York 1981.

9 Gutteberg, O. Measurements of atmospheric effects on satellite links at very low elevation angle, *AGARD Conference Proceedings*, No 346, 5-1 to 5-12, 1983.

10 Gutteberg, O. Eksperimenter med OTS-satellitten, *Telektronikk* 4/1981.

11 Gutteberg, O. *Low elevation propagation in high latitude regions*, TF report No 7/83, Norwegian Telecom Research, 1983.

12 Kokkila T. *Private communications*

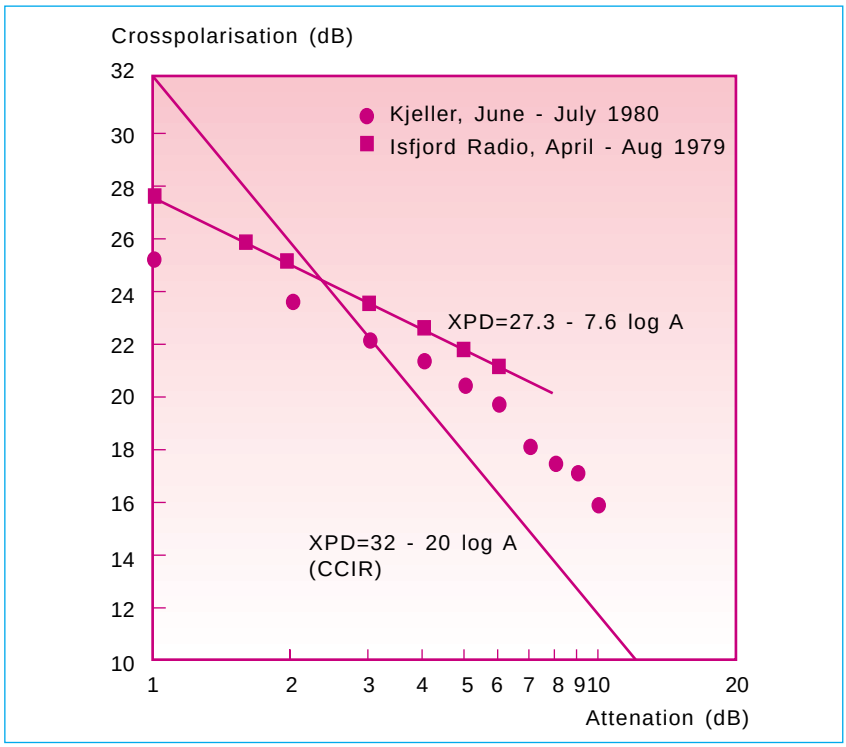

Figure 17 Crosspolarisation discrimination (XPD) as a function of co-polar attenuation (A)